Published in final edited form as:
Epilepsia. 2008 October ; 49(10): 1675–1685. doi:10.1111/j.1528-1167.2008.01613.x.

Characterization of osteopontin expression and function after status epilepticus

Karin Borges[*,†], **Marla Gearing**[‡], **Susan Rittling**[§], **Esben S. Sorensen**[¶], **Robert Kotloski**[#], **David T. Denhardt**[**], and **Raymond Dingledine**[†]

[*]Department of Pharmaceutical Sciences, Texas Tech Health Sciences Center, Amarillo, Texas, U.S.A.

[†]Department of Pharmacology, Emory University, Atlanta, Georgia, U.S.A.

[‡]Department of Pathology and Laboratory Medicine, Emory University, Atlanta, Georgia, U.S.A.

[§]Department of Cell Biology and Neuroscience, The Forsyth Institute, Boston, Massachusetts, U.S.A.

[¶]Protein Chemistry Laboratory, Department of Molecular Biology, University of Aarhus, Aarhus C, Denmark

[#]Department of Neurobiology, Duke University, Durham, North Carolina, U.S.A.

[**]Department of Cell Biology and Neuroscience, Rutgers University, Piscataway, New Jersey, U.S.A.

SUMMARY

Purpose—Osteopontin is a cytokine found in many tissues and plays a role in tissue injury and repair. This study had two goals: to characterize osteopontin expression after status epilepticus (SE), and to test the hypotheses that osteopontin affects the susceptibility to seizures or alters cell death and inflammation after SE.

Methods—Pilocarpine was used to induce SE in $OPN^{-/-}$ and $OPN^{+/+}$ mice to compare seizure susceptibility, neuropathological markers including real time PCR for inflammatory genes, and osteopontin immunohistochemistry. The effect of added osteopontin on excitotoxicity by N-methyl-D-aspartate in neuronal cultures of $ONP^{-/-}$ mice was determined.

Results—Neurons undergoing degeneration showed osteopontin immunoreactivity 2–3 days after SE. After 10 to 31 days degenerating axons in the thalamus were osteopontin-positive. The susceptibility to seizures of $OPN^{-/-}$ and $OPN^{+/+}$ mice in the pilocarpine, fluorothyl, and maximal electroshock models was similar. There were no significant differences in the extent of neuronal damage after pilocarpine-induced SE, the expression of several neuropathological markers or the

Address correspondence to Karin Borges, Ph.D., Department of Pharmaceutical Sciences, Texas Tech University Health Sciences, 1300 S Coulter, Amarillo, TX 79106, U.S.A. karin.borges@ttuhsc.edu.

Conflict of interest: We confirm that we have read the Journal's position on issues involved in ethical publication and affirm that this report is consistent with those guidelines. None of the authors has anything to disclose.

RNA levels of selected inflammatory genes. Recombinant and natural bovine osteopontin did not affect the extent of NMDA-induced cell death in $OPN^{-/-}$ mouse neuronal cultures.

Conclusion—We demonstrated that osteopontin is up-regulated in response to SE in distinct temporal sequences in the hippocampus, specifically in degenerating neurons and axons. However, osteopontin did not appear to regulate neurodegeneration or inflammation within the first 3 days after SE.

Keywords

Seizure; Pilocarpine; Inflammation; Axonal degeneration; Neuronal degeneration

Osteopontin (gene symbol spp1) is a highly glycosylated multifunctional phosphoprotein that influences adhesion, migration, cell survival, and inflammation (reviewed in Denhardt et al., 2001a, 2001b; Scatena et al., 2007). It is expressed in many tissues and cell types, such as bone, kidney, epithelial cells, arterial smooth muscles, inflammatory cells, certain brain areas, and in tumors. Osteopontin is usually secreted and is present in all body fluids but can also be found underneath the plasma membrane in association with the intracellular domain of CD44 (Zohar et al., 2000). Osteopontin is upregulated after injury in many peripheral tissues.

Osteopontin associates with the hyaluronin receptor CD44 and extracellular matrix molecules, including fibronectin, type I collagen, osteocalcin, and mediates cell attachment via its arginine-glycine-aspartate (RGD) sequence by binding to integrins. It also plays a role in cell migration and matrix reorganization after injury and wound healing (Liaw et al., 1998). Furthermore, osteopontin acts as a cytokine because it potently attracts macrophages and regulates secretion of cytokines from macrophages and T-cells. On the other hand, osteopontin can also limit inflammation by inhibition of matrix metalloproteinase 2 and inducible nitric oxide synthase (iNOS; reviewed in Denhardt et al., 2001b; Scatena et al., 2007).

Osteopontin is normally not detected in the healthy tel-encephalon and diencephalon, but has been found in other brain areas, such as the substantia nigra (Iczkiewicz et al., 2006; Schroeter et al., 2006), midbrain, brain stem, and the olfactory bulb (Shin et al., 1999) and in peripheral neurons (Ichikawa et al., 2001). Osteopontin has been reported to be upregulated in various brain disorders or after injury, e.g., after ischemia (Ellison et al., 1998; Wang et al., 1998; Lee et al., 1999; Choi et al., 2007), kainate-induced seizures (Kim et al., 2002), cryolesions (Shin et al., 2005), experimental autoimmune encephalomyelitis (EAE, Chabas et al., 2001), and spinal cord injury (Hashimoto et al., 2007). In human brain tissue osteopontin immunoreactivity was found in multiple sclerosis plaques (Chabas et al., 2001; Diaz-Sanchez et al., 2006) and in periventricular leukomalacia (Tanaka et al., 2000). Osteopontin appears to be protective against ischemic injury in the brain (Meller et al., 2005) and kidney (Noiri et al., 1999; Denhardt et al., 2001a, 2001b), but in contrast it also promotes inflammation and exacerbates autoinmmune diseases, such as EAE (Chabas et al., 2001).

In a microarray survey, we found that osteopontin was the most prominently upregulated among approximately 60 upregulated genes in the CA3 pyramidal cell layer 3 days after pilocarpine-induced status epilepticus (SE, Jim Doherty and Raymond Dingledine, unpublished). Given osteopontin's many roles in inflammation and tissue injury and its protective effects against ischemia, we hypothesized that osteopontin might alter neuropathological events after SE, including cell death and inflammation, or might affect the susceptibility to seizures. Here, we characterized osteopontin expression and its potential role after SE in a chronic seizure model.

METHODS

Mice and seizure models

The pilocarpine-injected CF1 mouse model used in this study was described earlier (Borges et al., 2003, 2004). Outbred CF1 mice (6–10 weeks old, 30–42 g) were obtained from Charles River (Wilmington, MA, U.S.A.). Mice deficient for osteopontin expression and their wild type counterparts were obtained from Dr. Susan Rittling ($OPN^{-/-}$ (SR) and $OPN^{+/+}$(SR); Rittling et al., 1998) and Dr. Lucy Liaw ($OPN^{-/-}$ (LL) and $OPN^{+/+}$(LL); Liaw et al., 1998). The $OPN^{-/-}$ and $OPN^{+/+}$ (SR) mice are derived from AB2.1 stem cells and are therefore a substrain of 129Sv mice from Jackson labs. $OPN^{-/-}$ and $OPN^{+/+}$ (LL) mice were bred into the 129/SvJ strain from Taconic Farms Inc. (Germantown, NY, U.S.A.; Liaw et al., 1998). All mice were housed under a 12 h light dark cycle with food and water ad libidum. Mice were injected with methylscopolamine and terbutaline (2 mg/kg each i.p. in 0.9% NaCl) to minimize peripheral side effects followed after 15–30 min by different doses of pilocarpine for CF1 mice (254–290 mg/kg, i.p.), $OPN^{-/-}$ and $OPN^{+/+}$ mice from Dr. Susan Rittling (255–310 mg/kg, i.p.) and Dr. Lucy Liaw (230–240 mg/kg, i.p.). Approximately 30% of injected mice experienced behavioral SE lasting about 5 h as defined by continuous seizure activity consisting mainly of whole body continuous clonic seizures. SE onset was defined as the onset of whole clonic body seizures that became continuous. SE severity was scored by the most severe seizure activity observed, with whole body clonic seizures scored as (1), severe whole body clonic seizures scored as (2), and tonic–clonic seizures or jumping scored as (3). We did not measure the end of SE, because behavioral assessment is highly subjective at this time point and electrographic SE can continue sporadically for at least 24 h (Kris Bough & Raymond Dingledine, unpublished). About 6 h after pilocarpine injection, all mice were injected with 0.5–0.8 ml 5% dextrose in lactate Ringer's solution (i.p.). Mice were fed moistened high-fat rodent chow and were monitored daily and injected with 5% dextrose in lactate Ringer's solution when needed. "Control" mice received terbutaline and methylscopolamine but no pilocarpine. CF1 mice that had experienced SE after repeated kainate injection were from a previous study (Borges et al., 2004). Briefly, kainate (5–20 mg/kg, i.p. in phosphate-buffered salt solution) was injected every 30 min until SE was reached. After 4–5 h of behavioral SE, seizures were terminated by injection of 25 mg/kg pentobarbital (i.p.).

For electroshock seizures one or two drops of local anesthetic (lidocaine, 1%) were placed in each conjunctiva of the animal. Approximately 30 s later, the animal was picked up gently and a cup electrode was placed over each cornea and current was administered through the

electrodes (Wahlquist Instrument Co., Salt Lake City, UT, U.S.A.). To induce maximal seizures, a stimulus of 200 mA at 60 Hz for 200 ms duration was administered. Seizure onset occurred virtually instantaneously with the onset of current flow. The durations of tonic hind limb flexion and tonic hind limb extension were recorded.

For the fluorothyl model, 18–26 g $OPN^{-/-}$ (SR) and $OPN^{+/+}$(SR) mice were placed individually into a clear plastic chamber (15 cm × 20 cm × 28 cm) and 20 ll/min fluorothyl was constantly dripped onto a filter paper placed on a platform near the top of the container. The volatile fluorothyl evaporates and the latencies required for the first myoclonic jerk and the first tonic-clonic seizure were timed.

All experiments were approved by the Institutional Animal Care and Use Committee (IACUC) of Emory University and conducted in accordance with its guidelines. Every effort was made to minimize animal suffering.

Immunohistochemistry and neuropathology

As described earlier (Borges et al., 2003) mice were sacrificed under deep isoflurane anesthesia, and their brains were removed and immersed in 4% paraformaldehyde fixative for at least 10 h. Brains were sliced coronally in 1–2 mm slices, dehydrated in a graded series of alcohols and xylenes and infiltrated with paraffin using an automated tissue processor (Shandon Hypercenter XP, Pittsburgh, PA, U.S.A.), then embedded in paraffin blocks. Eight lm sections were cut using a Shandon AS325 microtome.

To compare the extent of cell death in wild type and $OPN^{-/-}$ mice after pilocarpine-induced SE, sections were stained with hematoxylin. Healthy neurons could be easily distinguished from nonneuronal cells and injured neurons by their large size, medium-intensity staining and dark nucleoli. After SE, many pyramidal cells were shrunken and stained darkly or had disappeared at late time points.

The amount of hippocampal pyramidal cell damage in mice 2–3 days after pilocarpine-induced SE and control mice was assessed between −1.8 and −2.5 mm bregma (corresponding to mid-level hippocampal sections according to the atlas for C57BL/6 mice, Hof 2000) by a blinded investigator. The same investigator (KB) conducted all subjective ratings. The amount of damage in the hippocampal pyramidal CA1 and CA3 regions (a–c sectors considered together for CA3) were scored for each mouse on a 0–4 scale, by estimating in 25% increments the number of healthy cells remaining relative to control mice. Score 0 was given if the section was undistinguishable from control mice, i.e., the number of healthy neurons appeared normal, even if a few pyknotic cells were found. Score 1: >75% healthy pyramidal cells remaining, but with clear evidence of cell death; 2: 50–74%; 3: 25–49%; 4: <25% healthy pyramidal neurons remaining. The median score was calculated for each mouse from at least three or four hippocampal sections.

Eight-micron thick paraffin-embedded sections were immunohistochemically labeled as described (Gearing et al., 1993; Borges et al., 2003, 2004). Briefly, sections were deparaffinized in a series of xylenes and graded alcohols and were blocked with normal serum and then incubated with primary antibody, followed by biotinylated secondary

antibody and avidin-biotin-peroxidase complex (ABC Elite Kit, Vector Laboratories, Burlingame, CA, U.S.A.), the MOM kit (Vector Laboratories) or the Dako Envision System (Dako Corporation, Carpinteria, CA, U.S.A.) as instructed by the manufacturer. The chromagen used for color development was 3,3′-diaminobenzidine, and sections were counterstained with hematoxylin. For osteopontin staining, we used the monoclonal mouse 2A1 antibody (1:100) followed by the MOM kit (Vector Laboratories) or the rabbit LF-123 antibody (1:800, Fisher et al., 1995) with the Dako Envision System. For the amyloid precursor protein (APP) antibody (1:200, Boehringer Mannheim, GmbH, Mannheim, Germany), the biotinylated secondary antibody (1:8,000, Vector Laboratories) was followed by avidin-conjugated alkaline phosphatase, with nitroblue tetrazolium and 5-bromo, 4-chloro, 3-indolyl phosphate for color development with nuclear fast red counterstain. Other antibodies used to characterize the $OPN^{-/-}$ and $OPN^{+/+}$ mice after seizures were rabbit anti-cow glial fibrillary acidic protein (GFAP,1:500, Dako Corporation), rabbit anti-neuropeptide Y (NPY, 1:500, Bachem Americas, Inc., Torrance, CA, U.S.A.), goat anti-β2 microglobulin (M20, 1:200, Santa Cruz Biotechnology, Inc., Santa Cruz, CA, U.S.A.), and rat anti-CD44 antibodies (Km114, 1:100, and Im7, 1:50, both BD Pharmingen, San Jose, CA, U.S.A.); these were visualized with the ABC elite kit as described earlier (Borges et al., 2003, 2004). Positive and negative controls were included in each staining experiment. For all antibodies, negative controls included sections incubated in the absence of primary antibody. For the OPN antibodies, additional negative controls consisted of sections from $OPN^{-/-}$ mice 3 days after SE incubated in the presence of primary anti-body. Positive controls included sections after 1–3 days after SE or human brain sections known to stain with APP. All antibodies labeled specific structures and cell populations as described here or earlier.

Real-time PCR

Twenty-four hours after pilocarpine-induced SE, $OPN^{-/-}$ (SR) and $OPN^{+/+}$(SR) mice were decapitated under deep isoflurane anesthesia. Hippocampi were dissected out and frozen on dry ice. RNA was extracted using Tri reagent (Sigma-Aldrich, St. Louis, MO, U.S.A.) and treated with RNAse-free DNase on RNeasy columns (both Qiagen, Valencia, CA, U.S.A.). After elution, RNA was quantitated using Ribogreen and 250 ng of RNA wasreverse transcribed using oligo-dT primers and Superscript II (Invitrogen, Carlsbad, CA, U.S.A.). For real time PCR first strand cDNA from the equivalent of 3.6 ng RNA was reacted for 40 cycles with specific primer sets and SYBR Green PCR Master Mix (Applied Biosystems, Foster City, CA, U.S.A.) in an iCycler (Biorad, Hercules, CA, U.S.A.). All samples were run in duplicate. Real time primers were ordered from Integrated DNA Technologies, Inc. (Coralville, IA, U.S.A.; Table 1). All primer sets resulted in a single PCR product as judged from melt curves and had similar PCR efficiencies (94–114%) compared to glyceraldehyde 3-phosphate dehydrogenase (GAPDH) primers (105%). Threshold cycles were determined for GFAP, CD44, interleukin-1β (IL-1β), and iNOS and were normalized to the threshold cycles for GAPDH for every animal to account for small differences in cDNA starting concentrations ($\Delta Ct_{iRNA} = Ct_{iRNA} - Ct_{GAPDH}$). The fold increase of each inflammatory RNA (iRNA) was calculated for each animal 1 day after SE relative to the average amount of RNA found in six control animals (fold induction = 2 to the power of $\Delta Ct_{iRNA(SE)}$ − average $\Delta Ct_{iRNA(CON)}$).

Cell culture assays

E14 mouse neuronal cell cultures were prepared from timed pregnant $OPN^{-/-}$ (SR) mice. Briefly, the mother was sacrificed by isoflurane anesthesia followed by cervical dislocation. The embryos were removed and decapitated immediately. Forebrains were dissected out, the meninges removed, and neural cells were triturated to a single cell suspension in cold Neurobasal medium. Cells were seeded in Neurobasal medium with 1 mM glutamine supplemented with B27 (Invitrogen) at a density of about 75,000 cells/well into 24 well plates coated with 60 μg/ml poly-D-lysine. After 11–14 days in vitro, medium was partially removed for lactate dehydrogenase (LDH) measurements and 50–250 ng/ml mouse recombinant osteopontin (Sigma) or cow osteopontin isolated from milk (Sorensen & Petersen, 1993), or 250 ng/ml bovine serum albumin (BSA, Sigma) was added. After 2 h preincubation with osteopontin different concentrations of N-methyl-D-aspartate (NMDA) were added overnight for about 18 h. Neurobasal medium contains 400 μM glycine, so additional glycine was unnecessary. To quantify neuronal cell death the percentage of released LDH was essayed with an LDH cytotoxicity kit (Roche, Basel, Switzerland). Dose response curves were constructed with Origin software. The data from three different cultures were normalized by setting the maximum percentage of LDH release with NMDA and BSA to 100%.

Statistics

For parametric values we calculated mean and standard error of the mean (s.e.m.), and for scores we report the median. Unpaired two-tailed Student's *t*-tests were used to compare seizure thresholds in the fluorothyl and electroshock models, the induction of iRNAs in $OPN^{-/-}$ versus $OPN^{+/+}$ mice, and the log EC50s of NMDA-induced cell death with cow osteopontin versus BSA. The Mann–Whitney nonparametric test was used to compare SE severity scores and neuronal damage scores. One-way ANOVAs were employed to compare the threshold cycles for GAPDH among the four groups of mice and the log EC50s of NMDA-induced cell death with two different concentrations of recombinant osteopontin versus BSA. Graphpad Instat was employed for all statistical comparisons.

RESULTS

Osteopontin expression in degenerating neurons after SE

Osteopontin upregulation was initially found 3 days after pilocarpine-induced SE in a microarray study (Jim Doherty & Raymond Dingledine, unpublished). To assess the time course of osteopontin protein upregulation in this chronic epilepsy model two antibodies, mouse 2A1 and rabbit LF-123, were used to stain brains 1–31 days after pilocarpine-induced SE in CF1 mice (Figs. 1 and 2); both antibodies resulted in similar staining patterns (e.g., compare Figs. 1B3 and 1D). Osteopontin immunoreactivity was negative in untreated control mice (Fig. 1C), but appeared 1 day after pilocarpine-induced SE (Fig. 1A1, 1A2, and 1A3) and was strongest 2–3 days after SE (Figs. 1B1, 1B2, 1B3, and 1D). One day after SE only a few small cells, potentially microglia (Fig. 1A3), and some neurons identified by their nuclear morphology (Fig. 1A2), were labeled in the hippocampus and thalamus. Neuronal nuclei are large, stain light blue with the hematoxylin counterstain and contain several darker nucleoli. After 2–3 days extracellular matrix (Figs. 1B1, 1B2, 1B3, and 1D) and areas

showing neuronal damage, such as the hippocampus, thalamus, amygdala, and piriform cortex showed strong and abundant osteopontin labeling, specifically in small cells with dark nuclei, many resembling dying neurons (Figs. 1B1, 1B2, 1B3, and 1D) and some potentially representing microglia. Similarly, after SE induced by repeated kainate injections, cells in the pyramidal cell layer die (Borges et al., 2004) and small cells with dark nuclei were osteopontin-positive in the damaged hippocampal pyramidal cell layers (Fig. 1E). In some experiments, osteopontin-specific antibodies labeled astrocytes after 3 days of SE. However, this staining appears to be nonspecific because similar astrocyte labeling was found in $OPN^{-/-}$ mice after SE (not shown).

Osteopontin expression in degenerating axons after SE

Ten to 31 days after pilocarpine-induced-SE punctate osteopontin immunoreactivity was found in the thalamus in several nuclei, including the nucleus reuniens, ventromedial nucleus, lateral dorsal nucleus, the lateral geniculate nucleus (dorsal part), anterodorsal nucleus, and posterior complex of the thalamus (Figs. 2A and 2B). Previously, when assessing axonal degeneration with APP, a marker for degenerating axons (Kawarabayashi et al., 1991; Sherriff et al., 1994; Stone et al., 1999), we had found that these areas contained punctuate APP immunolabeling indicating axonal degeneration (Borges et al., 2003).

Direct comparisons of stainings for osteopontin and APP in adjacent sections (Fig. 2) show similar staining patterns, suggesting that degenerating axons express osteopontin.

Seizure susceptibility and neuropathology in OPN and OPN mice

First we investigated whether $OPN^{-/-}$ and $OPN^{+/+}$ mice exhibit differential vulnerability to seizures. In three different seizure models the seizure susceptibility was similar in osteopontin-deficient mice and their wild type counterparts. In the maximal electroshock model there were no significant differences in seizure duration between $OPN^{-/-}$ and $OPN^{+/+}$ (SR) mice (*t*-tests, Fig. 3A). Moreover, in the flurothyl model the latencies to onset of seizures were similar between both genotypes (Fig. 3B).

In the pilocarpine model, there were no apparent behavioral differences in time to SE onset, seizure behavior during SE, and duration of behavioral SE. The pilocarpine doses used in $OPN^{+/+}$ and $OPN^{-/-}$ mice that experienced SE and survived were similar: for the SR mice 280 ± 3.8 mg/kg in $OPN^{+/+}$ (n = 11) versus 265 ± 0.8 mg/kg in $OPN^{-/-}$ mice (n = 9) and for the LL mice 240 in $OPN^{+/+}$ (n = 3) versus 230 mg/kg in $OPN^{-/-}$ (n = 3). Onset to behavioral SE was similar among all groups, namely 41 ± 3 min in $OPN^{+/+}$ (SR, n = 11) versus 41 ± 4 min in $OPN^{-/-}$ mice (SR, n = 9) and 40 ± 11 min in $OPN^{+/+}$ (LL, n = 3) versus 47 ± 5 min in $OPN^{-/-}$ mice (LL,n = 3). During SE, most mice showed severe whole body convulsions (SE severity score 2), some showed tonic–clonic seizures or jumping (score 3) and some mice had whole body convulsions that were not classified as severe (score 1). The median SE severity score was 2 in each group, and there was no statistically significant difference in SE severity scores between $OPN^{-/-}$ and $OPN^{+/+}$ mice (Mann-Whitney test). Whole body clonic seizures slowed down in all genotypes after about 4.5 h of SE onset.

To assess whether osteopontin induction can alter the extent of neuronal damage after SE, we scored hematoxylin-stained sections obtained from mice 2–3 days after pilocarpine-inducedSEforthedamageinthehippocampalCA1and CA3pyramidalareas.Mostmicefrombothgenotypesshowed extensive (>75%) pyknosis in the pyramidal cell layers (Fig. 4). There were no significant differences in the cell damage scores between $OPN^{-/-}$ and $OPN^{+/+}$ mice (Mann-Whitney tests, Fig.5).

We confirmed that osteopontin was induced in $OPN^{+/+}$, but not $OPN^{-/-}$, mice from both sources 3 days after pilocarpine-induced SE by immunohistochemistry (not shown). To investigate whether there are other neuropathologic differences between osteopontin-deficient and expressing mice we compared the immunolabeling for various pathological markers that are upregulated in the pilocarpine model (e.g., Borges et al., 2003, 2004). We observed no obvious changes in staining patterns for NPY, β2-microglobulin, GFAP, and CD44 3 days after SE in $OPN^{-/-}$ and $OPN^{+/+}$ mice from SR and LL. After SE in both genotypes, NPY labeling was induced in mossy fibers. In areas showing neuronal damage β2-microglobulin labeling appeared in small cells suggestive of activated microglia. GFAP staining increased in astrocytes after SE indicating astrogliosis. CD44 staining appeared in the supragranular layer above the dentate granule cell layer and the extracellular matrix as previously described (Borges et al., 2004).

Regulation of the RNA of inflammatory mediators after SE

To test the hypothesis that the induction of osteopontin after SE regulates expression of inflammatory molecules, we compared the RNA levels of iNOS, GFAP, IL-1β, and CD44 1 day after pilocarpine-induced SE in $OPN^{-/-}$ (SR) and $OPN^{+/+}$(SR) mice relative to control mice that had not received pilocarpine. For real time PCR all samples were normalized to GAPDH threshold cycles, which were not significantly different among treatment groups (25.0 ± 0.3 in control $OPN^{+/+}$ mice and 24.4 ± 0.4 after SE, 24.3 ± 0.2 in control $OPN^{-/-}$ mice and 24.4 ± 0.5 after SE, n 6 mice in each group, one-way ANOVA), indicating that=SE did not change GAPDH levels. iRNAs were elevated between 2-(iNOS) and 102-fold (CD44) 1 day after SE (Fig. 6A). IL-1β showed a trend of a more pronounced upregulation in osteopontin-deficient mice relative to wild type mice (*t*-test, p = 0.138). Interestingly, the amounts of hippocampal IL-1β RNA showed a trend of being 4.0 ± 1.4-fold higher in control $OPN^{-/-}$ compared to wild type mice (Fig. 6B, n = 5–6; p = 0.16, *t*-test), while 1 day SE the amounts were after more similar. All other RNA levels were similar in control $OPN^{-/-}$ (SR) and $OPN^{+/+}$(SR) mice and induced to a similar degree in wild type and $OPN^{-/-}$ mice (n = 6, *t*-tests).

Osteopontin does not protect against NMDA excitotoxicity

Hippocampal neuronal death after pilocarpine-induced SE is mediated in large part by NMDA receptor activation (e.g., Rice & DeLorenzo, 1998; Ebert et al., 2002; Brandt et al., 2003). Therefore, to test the hypothesis that osteopontin is neuroprotective when present at the time of insult we compared the NMDA-induced toxicity in osteopontin-deficient neuronal cell cultures pretreated with BSA or two different sources of osteopontin, natural cow osteopontin or recombinant mouse osteopontin. There were no differences in the

maximum amount of LDH release or the log EC50 for NMDA-induced cell death with osteopontin from the two sources relative to BSA (Fig. 7, ANOVA and *t*-test).

DISCUSSION

Expression of osteopontin in damaged neurons and axons

A major finding of this study is that osteopontin is strongly upregulated in degenerating neurons and axons after SE. Similarly, damaged neurons were labeled with the same 2A1 antibody in brain cryolesions (Shin et al., 2005) and with another antibody in the rat EAE model (Chabas et al., 2001). In tissue from patients with periventricular leukomalacia and multiple sclerosis, damaged axons were also osteopontin-positive (Tanaka et al., 2000; Chabas et al., 2001; Diaz-Sanchez et al., 2006). Moreover, the in situ hydridization of osteopontin RNA after transient global ischemia in the rat hippocampus is consistent with osteopontin expression in damaged neurons (Lee et al., 1999). Osteopontin expression in dying cells and axons may attract and activate microglia/macrophages to clean up the injured tissue, as osteopontin appears to do in injured peripheral tissues (Denhardt et al., 2001a; Persy et al., 2003).

Usually, osteopontin upregulation is reported in microglia and often astrocytes in brain injury models (Ellison et al., 1998; Wang et al., 1998; Hashimoto et al., 2003; Shin et al., 2005; Diaz-Sanchez et al., 2006; Choi et al., 2007; Iczkiewicz et al., 2007). We did not observe any convincing osteopontin labeling of microglia after SE, although some small cells were osteopontin-positive and may represent microglia, especially in the areas of neuronal damage. However, clear osteopontin labeling of microglial-like processes or amoeboid microglia found at 10 days in the hilus (Borges et al., 2003) was not observed. Lack of osteopontin-staining in activated microglial cells was also found in periventricular leukomalacia (Tanaka et al., 2000). After kainate-induced seizures only amoeboid microglia, but not other microglial subtypes, were osteopontin-positive (Kim et al., 2002), indicating that not all stages of activated microglia are osteopontin-positive.

Osteopontin expression in astrocytes after SE is doubtful, because we found astrocyte labeling in osteopontin-deficient mice after SE despite the use of the MOM kit, which is intended to suppress nonspecific antibody binding. To our knowledge most other researchers have not performed negative controls that included immunostaining of osteopontin-deficient mice. On the other hand, there is convincing evidence for astroglial osteopontin expression after ischemia in rats from osteopontin in situ hybridization coupled with GFAP immunohistochemistry (Choi et al., 2007), suggesting that astrocytes express osteopontin under certain conditions.

Osteopontin and seizure threshold

We did not find a difference in seizure susceptibility of $OPN^{-/-}$and $OPN^{+/+}$ mice in the pilocarpine, fluorothyl seizure, and maximal electroshock models indicating that in normal mice osteopontin does not affect the sensitivity to seizures. We cannot rule out the possibility that osteopontin regulates neuronal excitability and seizure susceptibility in mice

after an insult or in chronically epileptic mice. Further studies are warranted to investigate this issue.

Osteopontin and neuroprotection

We did not find a neuroprotective role of osteopontin in vitro or 1–3 days after SE in vivo, although osteopontin has been found to be protective in brain ischemia, spinal cord injury, and in the MPTP Parkinson's disease model (Meller et al., 2005; Schroeter et al., 2006; Hashimoto et al., 2007; Maetzler et al., 2007). This discrepancy may be explained by the shorter time course of our experiments compared to the above-mentioned studies. After ischemic cortical stroke, no difference in lesion volume was found in the cortex, but there was an increase in delayed thalamic neurodegeneration 14 days later in wild type mice relative to osteopontin-deficient mice (Schroeter et al., 2006). Similarly, reduced neurodegeneration in the MPTP Parkinson's disease model was apparent in osteopontin-deficient mice after 3 weeks (Maetzler et al., 2007). After spinal cord injury, osteopontin-deficient mice exhibited greater tissue damage compared to wild type mice only at later stages (42 days), but not 24 h after injury (Hashimoto et al., 2007). It is likely that osteopontin may need to be present during the time of injury to effectively protect the brain. For example, intracerebroventricular injection of osteopontin protected against acute cortical ischemic injury (Meller et al., 2005). Based on this knowledge and the fact that osteopontin expression peaked around 3 days, but not 1 day after SE, it would be worthwhile to investigate long-term changes after SE in osteopontin-deficient mice, including neuronal sprouting, rewiring, and spontaneous seizure behavior.

We preincubated rat cortical cultures from $OPN^{-/-}$ mice with recombinant and native cow milk osteopontin for 2 h and found no neuroprotective effects against NMDA challenge. In contrast 24 h preincubation with recombinant osteopontin from a different source protected against oxygen and glucose deprivation at similar concentrations (Meller et al., 2005). It seems that the time of preincubation in our experiments was sufficient, because intracerebroventricular injection of osteopontin immediately before ischemia induced by transient middle cerebral artery occlusion protected against acute cortical injury. It would be worthwhile to investigate whether our sources of osteopontin or our injury model is responsible for the lack of effect.

Inflammation and wound healing

Osteopontin-neutralizing antibodies and genetic ablation of osteopontin greatly impair macrophage recruitment in several models of inflammation, e.g., in the kidney (reviewed in Scatena et al., 2007). Moreover, osteopontin regulates macrophage activity. Here, we did not observe any changes in the levels of RNAs of inflammatory molecules or in β2-microglobulin labeling, which labels microglia/macrophages. Local microglia present in the brain may be able to carry out invading macrophage functions and microglia appear to be activated without osteopontin as evidenced by β2-microglobulin expression and induction of iNOS and IL-1β RNA in the $OPN^{-/-}$ mouse. Again, it is possible that at later stages after SE there is a difference in the inflammatory response.

Interestingly, in ischemic cortex IL-1β was upregulated about 50-fold in osteopontin-deficient mice, but only 20-fold in wild type mice after 24 h (Schroeter et al., 2006). A very similar difference in induction was observed here 1 day after SE in hippocampus. These parallel observations may indicate that a more pronounced IL-1β induction after SE or ischemia may compensate for the loss of osteopontin in $OPN^{-/-}$ mice.

Taken together, our findings indicate that osteopontin is upregulated in degenerating neurons and axons peaking 3–10 days after SE, but no differences in cell damage and inflammation were detected between osteopontin-deficient and wild type mice at 1–3 days after SE. We conclude that rather than regulating short-term events after SE, it is more likely that osteopontin regulates long-term processes, including tissue healing, neuronal sprouting, rewiring, and possibly spontaneous seizures.

Acknowledgments

We are grateful to the Epilepsy Foundation for funding (KB) and National Institutes of Health Grant 5U54-HG003918 (R.D.). We thank Lucy Liaw for providing $OPN^{-/-}$ and $OPN^{+/+}$ mice, Aaron Kowalski and Larry Fisher for osteopontin antibodies, James McNamara for help with the electroshock tests, Kroshona Tabb for help with the fluorothyl test, Valerie Boss and James P. O'Callaghan for sharing real time primer sequences, Dayna McDermott for help with the immunohistochemistry and Renee Shaw for help with RNA isolations and real-time PCR.

REFERENCES

Borges K, Gearing M, McDermott DL, Smith AB, Almonte AG, Wainer BH, Dingledine R. Neuronal and glial pathological changes during epileptogenesis in the mouse pilocarpine model. Exp Neurol. 2003; 182:21–34. [PubMed: 12821374]

Borges K, McDermott DL, Dingledine R. Reciprocal changes of CD44 and GAP-43 expression in the dentate gyrus inner molecular layer after status epilepticus in mice. Exp Neurol. 2004; 188:1–10. [PubMed: 15191797]

Brandt C, Potschka H, Loscher W, Ebert U. N-methyl-D-aspartate receptor blockade after status epilepticus protects against limbic brain damage but not against epilepsy in the kainate model of temporal lobe epilepsy. Neuroscience. 2003; 118:727–740. [PubMed: 12710980]

Chabas D, Baranzini SE, Mitchell D, Bernard CC, Rittling SR, Denhardt DT, Sobel RA, Lock C, Karpuj M, Pedotti R, Heller R, Oksenberg JR, Steinman L. The influence of the proinflammatory cytokine, osteopontin, on autoimmune demyelinating disease. Science. 2001; 294:1731–1735. [PubMed: 11721059]

Choi JS, Kim HY, Cha JH, Choi JY, Lee MY. Transient microglial and prolonged astroglial upregulation of osteopontin following transient forebrain ischemia in rats. Brain Res. 2007; 1151:195–202. [PubMed: 17395166]

Denhardt DT, Giachelli CM, Rittling SR. Role of osteopontin in cellular signaling and toxicant injury. Annu Rev Pharmacol Toxicol. 2001a; 41:723–749. [PubMed: 11264474]

Denhardt DT, Noda M, O'Regan AW, Pavlin D, Berman JS. Osteopontin as a means to cope with environmental insults: regulation of inflammation, tissue remodeling, and cell survival. J Clin Invest. 2001b; 107:1055–1061. [PubMed: 11342566]

Diaz-Sanchez M, Williams K, DeLuca GC, Esiri MM. Protein co-expression with axonal injury in multiple sclerosis plaques. Acta Neuropathol (Berl). 2006; 111:289–299. [PubMed: 16547760]

Ebert U, Brandt C, Loscher W. Delayed sclerosis, neuro protection, and limbic epileptogenesis after status epilepticus in the rat. Epilepsia. 2002; 43(Suppl 5):86–95. [PubMed: 12121301]

Ellison JA, Velier JJ, Spera P, Jonak ZL, Wang X, Barone FC, Feuerstein GZ. Osteopontin and its integrin receptor alpha(v)beta3 are upregulated during formation of the glial scar after focal stroke. Stroke. 1998; 29:1698–1706. discussion 1707. [PubMed: 9707214]

Fisher LW, Stubbs JT 3rd, Young MF. Antisera and cDNA probes to human and certain animal model bone matrix noncollagenous proteins. Acta Orthop Scand Suppl. 1995; 266:61–65. [PubMed: 8553864]

Gearing M, Wilson RW, Unger ER, Shelton ER, Chan HW, Masters CL, Beyreuther K, Mirra SS. Amyloid precursor protein (APP) in the striatum in Alzheimer's disease: an immunohistochemical study. J Neuropathol Exp Neurol. 1993; 52:22–30. [PubMed: 7678853]

Hashimoto M, Koda M, Ino H, Murakami M, Yamazaki M, Moriya H. Upregulation of osteopontin expression in rat spinal cord microglia after traumatic injury. J Neurotrauma. 2003; 20:287–296. [PubMed: 12820683]

Hashimoto M, Sun D, Rittling SR, Denhardt DT, Young W. Osteopontin-deficient mice exhibit less inflammation, greater tissue damage, and impaired locomotor recovery from spinal cord injury compared with wild-type controls. J Neurosci. 2007; 27:3603–3611. [PubMed: 17392476]

Hof, P.; Young, WG.; Bloom, FE.; Belichenko, PV.; Celio, MR. Comparative cytoarchitonic atlas of the C57BL/6 and 129/Sv mouse brains. Elsevier; New York: 2000.

Ichikawa H, Yamashita K, Takano-Yamamoto T, Sugimoto T. Osteopontin-immunoreactivity in the rat trigeminal ganglion and trigeminal sensory nuclei. Brain Res. 2001; 919:147–154. [PubMed: 11689172]

Iczkiewicz J, Jackson MJ, Smith LA, Rose S, Jenner P. Osteopontin expression in substantia nigra in MPTP-treated primates and in Parkinson's disease. Brain Res. 2006; 1118:239–250. [PubMed: 16962083]

Iczkiewicz J, Rose S, Jenner P. Osteopontin expression in activated glial cells following mechanical- or toxin-induced nigral dopaminergic cell loss. Exp Neurol. 2007; 207:95–106. [PubMed: 17643430]

Kawarabayashi T, Shoji M, Harigaya Y, Yamaguchi H, Hirai S. Expression of APP in the early stage of brain damage. Brain Res. 1991; 563:334–338. [PubMed: 1786548]

Kim SY, Choi YS, Choi JS, Cha JH, Kim ON, Lee SB, Chung JW, Chun MH, Lee MY. Osteopontin in kainic acid-induced microglial reactions in the rat brain. Mol Cells. 2002; 13:429–435. [PubMed: 12132583]

Lee MY, Shin SL, Choi YS, Kim EJ, Cha JH, Chun MH, Lee SB, Kim SY. Transient upregulation of osteopontin mRNA in hippocampus and striatum following global forebrain ischemia in rats. Neurosci Lett. 1999; 271:81–84. [PubMed: 10477107]

Liaw L, Birk DE, Ballas CB, Whitsitt JS, Davidson JM, Hogan BL. Altered wound healing in mice lacking a functional osteopontin gene (spp1). J Clin Invest. 1998; 101:1468–1478. [PubMed: 9525990]

Maetzler W, Berg D, Schalamberidze N, Melms A, Schott K, Mueller JC, Liaw L, Gasser T, Nitsch C. Osteopontin is elevated in Parkinson's disease and its absence leads to reduced neurodegeneration in the MPTP model. Neurobiol Dis. 2007; 25:473–482. [PubMed: 17188882]

Meller R, Stevens SL, Minami M, Cameron JA, King S, Rosenzweig H, Doyle K, Lessov NS, Simon RP, Stenzel-Poore MP. Neuroprotection by osteopontin in stroke. J Cereb Blood Flow Metab. 2005; 25:217–225. [PubMed: 15678124]

Noiri E, Dickman K, Miller F, Romanov G, Romanov VI, Shaw R, Chambers AF, Rittling SR, Denhardt DT, Goligorsky MS. Reduced tolerance to acute renal ischemia in mice with a targeted disruption of the osteopontin gene. Kidney Int. 1999; 56:74–82. [PubMed: 10411681]

Persy VP, Verhulst A, Ysebaert DK, De Greef KE, De Broe ME. Reduced postischemic macrophage infiltration and interstitial fibrosis in osteopontin knockout mice. Kidney Int. 2003; 63:543–553. [PubMed: 12631119]

Phillipson M, Henriksnas J, Holstad M, Sandler S, Holm L. Inducible nitric oxide synthase is involved in acid-induced gastric hyperemia in rats and mice. Am J Physiol Gastrointest Liver Physiol. 2003; 285:G154–162. [PubMed: 12646421]

Rice AC, DeLorenzo RJ. NMDA receptor activation during status epilepticus is required for the development of epilepsy. Brain Res. 1998; 782:240–247. [PubMed: 9519269]

Rittling SR, Matsumoto HN, McKee MD, Nanci A, An XR, Novick KE, Kowalski AJ, Noda M, Denhardt DT. Mice lacking osteopontin show normal development and bone structure but display altered osteoclast formation in vitro. J Bone Miner Res. 1998; 13:1101–1111. [PubMed: 9661074]

Scatena M, Liaw L, Giachelli CM. Osteopontin. A Multifunctional Molecule Regulating Chronic Inflammation and Vascular Disease. Arterioscler Thromb Vasc Biol. 2007; 27:2302–2309. [PubMed: 17717292]

Schroeter M, Zickler P, Denhardt DT, Hartung HP, Jander S. Increased thalamic neurodegeneration following ischaemic cortical stroke in osteopontin-deficient mice. Brain. 2006; 129:1426–1437. [PubMed: 16636021]

Sherriff FE, Bridges LR, Sivaloganathan S. Early detection of axonal injury after human head trauma using immunocytochemistry for beta-amyloid precursor protein. Acta Neuropathol. 1994; 87:55–62. [PubMed: 8140894]

Shin SL, Cha JH, Chun MH, Chung JW, Lee MY. Expression of osteopontin mRNA in the adult rat brain. Neurosci Lett. 1999; 273:73–76. [PubMed: 10505619]

Shin T, Ahn M, Kim H, Moon C, Kang TY, Lee JM, Sim KB, Hyun JW. Temporal expression of osteopontin and CD44 in rat brains with experimental cryolesions. Brain Res. 2005; 1041:95–101. [PubMed: 15804504]

Sorensen ES, Petersen TE. Purification and characterization of three proteins isolated from the proteose peptone fraction of bovine milk. J Dairy Res. 1993; 60:189–197. [PubMed: 8320368]

Stone JR, Walker SA, Povlishock JT. The visualization of a new class of traumatically injured axons through the use of a modified method of microwave antigen retrieval. Acta Neuropathol (Berl). 1999; 97:335–345. [PubMed: 10208272]

Tanaka F, Ozawa Y, Inage Y, Deguchi K, Itoh M, Imai Y, Kohsaka S, Takashima S. Association of osteopontin with ischemic axonal death in periventricular leukomalacia. Acta Neuropathol (Berl). 2000; 100:69–74. [PubMed: 10912922]

Wang X, Louden C, Yue TL, Ellison JA, Barone FC, Solleveld HA, Feuerstein GZ. Delayed expression of osteopontin after focal stroke in the rat. J Neurosci. 1998; 18:2075–2083. [PubMed: 9482794]

Wang H, Zhan Y, Xu L, Feuerstein GZ, Wang X. Use of suppression subtractive hybridization for differential gene expression in stroke: discovery of CD44 gene expression and localization in permanent focal stroke in rats. Stroke. 2001; 32:1020–1027. [PubMed: 11283406]

Zohar R, Suzuki N, Suzuki K, Arora P, Glogauer M, McCulloch CA, Sodek J. Intracellular osteopontin is an integral component of the CD44-ERM complex involved in cell migration. J Cell Physiol. 2000; 184:118–130. [PubMed: 10825241]

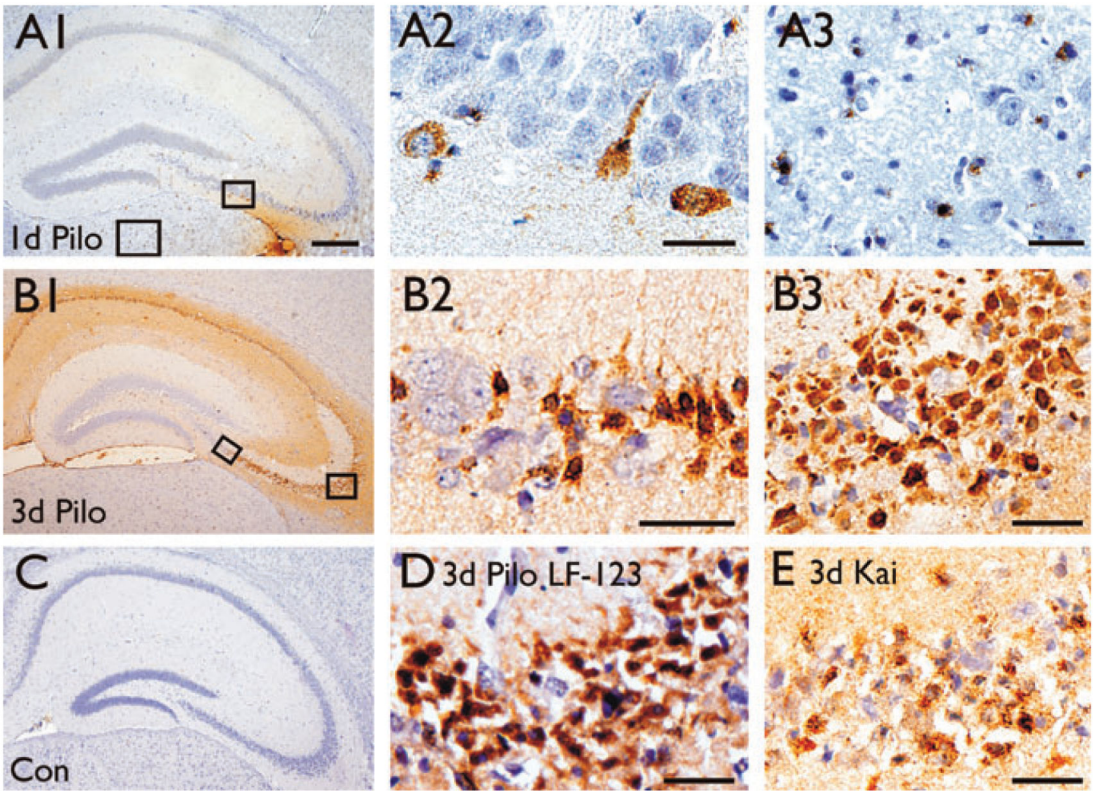

Figure 1.

Osteopontin expression in the hippocampus 1–3 days after SE. Osteopontin immunohistochemistry using 2A1 (**A–C** and **E**) and LF-123 (**D**) antibodies are shown for brain sections 1 (**A1–A3**) and 3 days after pilocarpine-(**B1–B3, D**) and 3 days after kainate-(**E**) induced SE in comparison to a control CF1 mouse (**C**). One day after pilocarpine-induced SE there is little staining in the hippocampus restricted to some cells with neuronal morphology (**A2**) and some small cells in the thalamus (**A3**). (**B**) Three days after pilocarpine-induced SE neurons with healthy morphology are not stained (**B2**), while smaller cells with the morphology of pyknotic neurons are stained in the pyramidal cell layers (**B3, D**). Note that the immunolabelings with the 2A1 (**B3**) and LF-123 (**D**) antibodies in the CA3b area are similar. D shows less robust but similar labeling in the CA3b area 3 days after kainate-induced SE. The scale bar is 500 μm for A1, B1, and C. All other scale bars = 50 μm

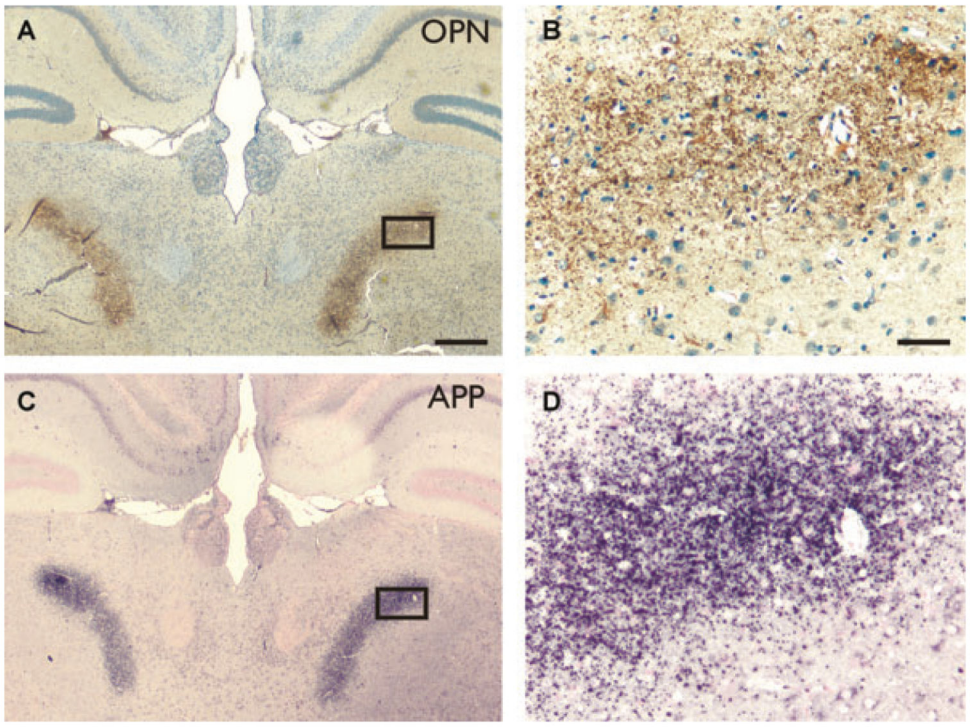

Figure 2.

Osteopontin labels degenerating axons. Osteopontin (2A1 antibody, **A, B**) and APP (**C, D**) immunolabeling 10 days after pilocarpine-induced SE in the posterior complex of the thalamus in adjacent sections. Scale bar is 500 μm for A and B and 50 μm for C and D. *Epilepsia* © ILAE

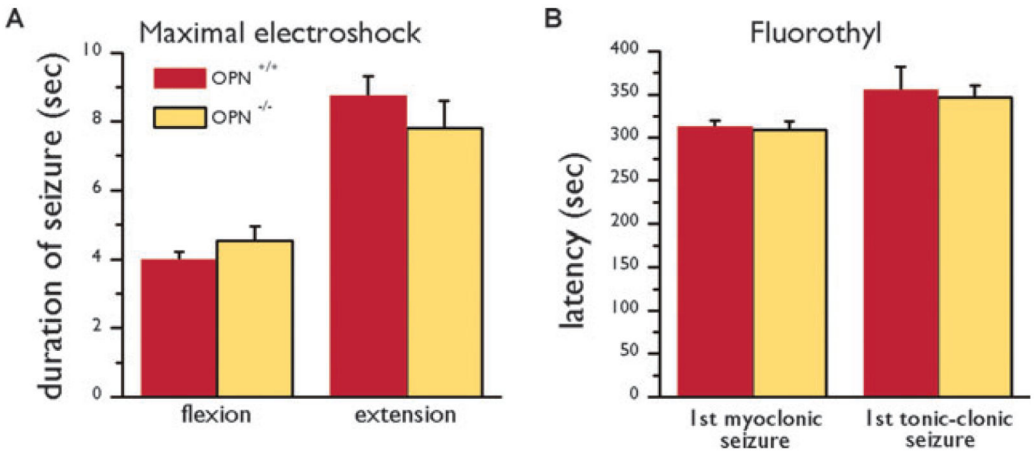

Figure 3.

Behavior of $OPN^{-/-}$ (SR) and $OPN^{+/+}$ (SR) mice in seizure models. (**A**) The average (± s.e.m.) durations of hind limb flexion and extension after maximal electroshock are compared in $OPN^{+/+}$ (red bars) and $OPN^{-/-}$ mice (yellow bars). (**B**) The latencies until the first jerk and first tonic-clonic seizure in the fluorothyl model are compared in $OPN^{+/+}$ (red bars) and $OPN^{-/-}$ mice (yellow bars). There were no significant differences (*t*-tests).

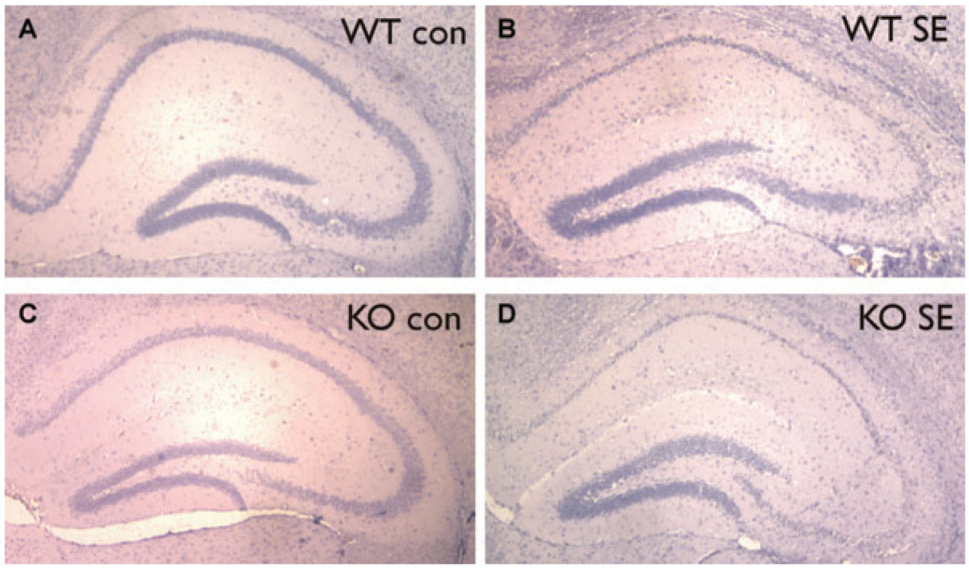

Figure 4.

Neuronal damage in $OPN^{-/-}$ and $OPN^{+/+}$ (SR) mice after pilocarpine-induced SE. Representative hematoxylin-stained hippocampal sections are shown of $OPN^{+/+}$ (**A, B**) and $OPN^{-/-}$ (**C, D**) mice without (**A, C**) and 3 days after pilocarpine-induced SE (**B, D**).

Epilepsia © ILAE

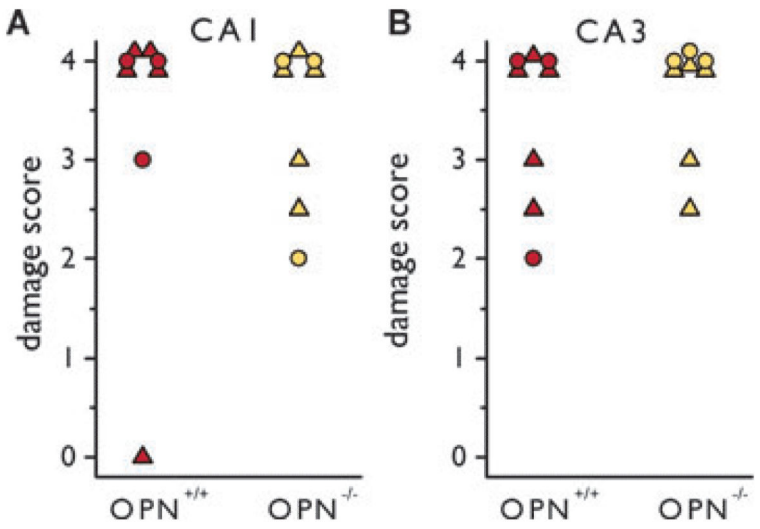

Figure 5.

Neuronal damage scores in $OPN^{-/-}$ and $OPN^{+/+}$ (SR) mice after pilocarpine-induced SE. The scores of hematoxylin-stained sections 2–3 days after SE from $OPN^{-/-}$ and $OPN^{+/+}$ mice are shown for the hippocampal CA1 (**A**) and CA3 (**B**) pyramidal areas. Mice from SR are depicted as colored triangles and mice from LL as colored circles. There are no significant differences (Mann-Whitney tests).

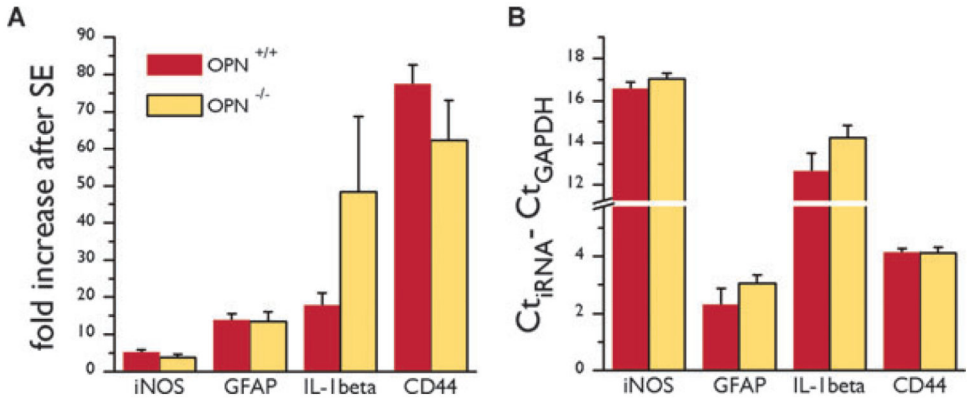

Figure 6.

Induction of iRNAs 1 day after pilocarpine-induced SE in $OPN^{-/-}$ (SR) and $OPN^{+/+}$ (SR) mice. (**A**) The average and s.e.m. of the fold increase of iRNA species measured by real time PCR is shown. (**B**) Threshold cycles for iRNA normalized to the threshold cycles for GAPDH for every animal ($Ct_{iRNA} - Ct_{GAPDH}$) are shown for control mice. There were no significant differences (*t*-tests, n = 5–6 mice per group).

Epilepsia © ILAE

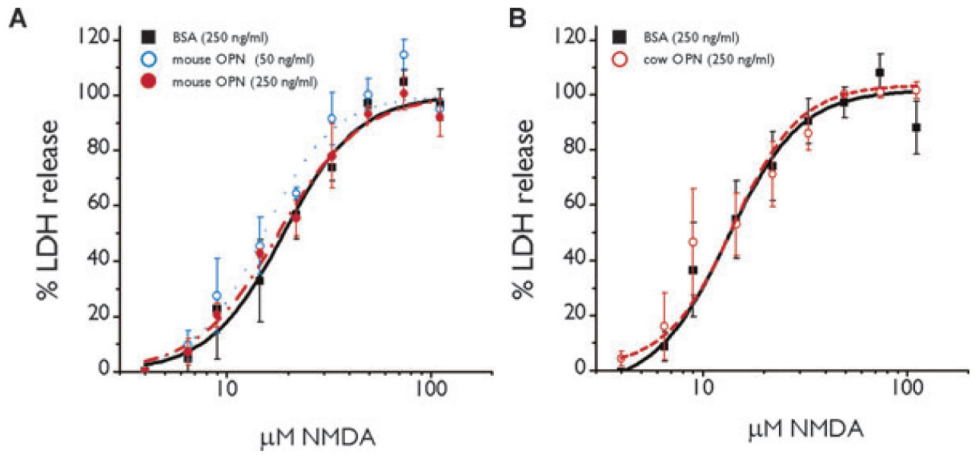

Figure 7.

Osteopontin does not protect against excitotoxicity. The average of the percentage of LDH release as a measure of neuronal cell death is shown relative to the concentration of NMDA applied for 18 h (**A**) The EC50s for NMDA are similar for 250 ng/ml BSA (black squares; 19.0 ± 1.4 μM), 50 ng/ml (blue open circles; 15.3 ± 1.1 μM) and 250 ng/ml mouse osteopontin (filled red circles; 18.0 ± 1.4 μM, ANOVA). (**B**) In another set of three experiments the EC50s for NMDA are similar for 250 ng/ml BSA (black squares; 13.3 ± 1.1 μM), and 250 ng/ml cow osteopontin (open red circles; 14.1 ± 2.2 μM, *t*-test).

Table 1

Real time PCR primer sequences

Primer	Sequence (5 to 3)	TAnneal	Source
GAPDH	F cagtatgactctacccacggca	61 °C	Valerie Boss, personal communication
	R ccttctccatggtggtgaagac		
iNOS	F cagctgggctgtacaaacctt	56°C	Phillipson et al., 2003
	R cattggaagtgaagcgtttcg		
GFAP	F gctagctacatcgagaaggtc	60°C	James P. O'Callaghan, personal communication
	R tccagcctcaggttggtttca		
IL1-beta	F Gcagcacatcaacaagagcttca	60°C	This study
	R tctaatgggaacgtcacacaccag		
CD44	F cagcctactggagatcaggatga	61 °C	Wang et al., 2001
	R ggagtccttggatgagtctcga		

Note: The sequences of all real time PCR primers (5′ to 3′) are shown with the annealing temperature used during PCR and the sources forthe sequences.